scientific reports

Check for updates

OPEN

Colossal figure of merit and compelling HER catalytic activity of holey graphyne

Muhammad Sajjad[1,4], Surabhi Suresh Nair[1,4], Yarjan Abdul Samad[2,3] & Nirpendra Singh[1]✉

Herein, we have conducted a comprehensive study to uncover the thermal transport properties and hydrogen evolution reaction catalytic activity of recently synthesized holey graphyne. Our findings disclose that holey graphyne has a direct bandgap of 1.00 eV using the HSE06 exchange–correlation functional. The absence of imaginary phonon frequencies in the phonon dispersion ensures its dynamic stability. The formation energy of holey graphyne turns out to be − 8.46 eV/atom, comparable to graphene (− 9.22 eV/atom) and *h*-BN (− 8.80 eV/atom). At 300 K, the Seebeck coefficient is as high as 700 μV/K at a carrier concentration of 1×10^{10} cm^{-2}. The predicted room temperature lattice thermal conductivity (κ_l) of 29.3 W/mK is substantially lower than graphene (3000 W/mK) and fourfold smaller than C_3N (128 W/mK). At around 335 nm thickness, the room temperature κ_l suppresses by 25%. The calculated *p*-type figure of merit (*ZT*) reaches a maximum of 1.50 at 300 K, higher than that of holey graphene (*ZT* = 1.13), γ-graphyne (*ZT* = 0.48), and pristine graphene ($ZT = 0.55 \times 10^{-3}$). It further scales up to 3.36 at 600 K. Such colossal *ZT* values make holey graphyne an appealing *p*-type thermoelectric material. Besides that, holey graphyne is a potential HER catalyst with a low overpotential of 0.20 eV, which further reduces to 0.03 eV at 2% compressive strain.

Rapidly growing population and infrastructure development are behind the rising energy demand, which will further increase from 23 Terawatts in 2030 to 30 Terawatts in 2050[1]. According to the Global Renewable Energy Community (REN21) statistics, nearly 80% of the total energy relies on conventional energy resources and renewable energy sources add only the rest 20%[2]. An excessive dependence on fossil fuels causes global warming and destructive environmental issues[3]. There has been a worldwide push to find sustainable and clean alternatives to fossil fuels to counter such problems[4]. Among the natural renewable energy sources, hydrogen is an ideal sustainable energy source due to its high energy density and environmentally benign[5]. However, precious and less abundant metal-based catalysts have been used for hydrogen production[6], impeding their widespread utilization[7]. Therefore, exploring novel and metal-free catalysts is a viable route for the mass production of hydrogen[8,9]. Thermoelectric generators are also excellent alternatives for clean and renewable energy resources, considering the abundance of waste heat accompanied by infrequent maintenance and long device life, as no moving parts are involved in the technology[10,11]. Although Bi_2Te_3 has been widely used in thermoelectric generators, the toxicity and scarcity of tellurium restrict their usage[12]. In addition, bipolar conduction suppresses the figure of merit of Bi_2Te_3 above 450 K due to its narrow bandgap[12]. Hence abundant and non-toxic materials with reasonable bandgap would be an optimal choice.

Since the experimental realization of graphene[13], tremendous attention has been devoted to other two-dimensional (2D) carbon allotropes due to their peculiar physical properties[14], topological states[15], massless Dirac cones[16,17], and semiconducting behavior[18,19]. Porous nitrogenated holey graphene[20], polyaniline[21], phagraphene[22], naphyne[23], graphtetrayne[24], and biphenylene[25] are a few examples of experimentally synthesized 2D carbon allotropes.

Among these, graphyne, with varying *sp* and sp^2 hybridized carbon atoms constitutes one of the biggest families of graphene allotropes[26]. They possess exceptional flexibility, high carrier mobility, a Dirac cone characterized electronic band structure, efficient adsorption of ions and molecular selectivity due to porous structures, and reduced thermal conductivity due to acetylenic bonds with *sp* state[27–32]. Recently, the bottom-up technique has been employed to synthesize an ultrathin 2D carbon allotrope named holey graphyne[33]. The nanosheet shows

[1]Department of Physics, Khalifa University of Science and Technology, 127788 Abu Dhabi, United Arab Emirates. [2]Department of Aerospace Engineering, Khalifa University of Science and Technology, 127788 Abu Dhabi, United Arab Emirates. [3]Cambridge Graphene Centre, Department of Engineering, University of Cambridge, Cambridge, UK. [4]These authors contributed equally: Muhammad Sajjad and Surabhi Suresh Nair. ✉email: nirpendra.singh@ku.ac.ae

excellent mechanical, thermal, and dynamic stability. Unlike graphene, it is a direct bandgap semiconductor with high carrier mobility (promising for applications in optoelectronics) and possesses *sp* and sp^2 hybridized carbon atoms uniformly distributing the porous architectures (favorable for gas separation, water desalination, energy storage, and catalysis)[34]. Holey graphyne may also be considered an anchoring material in metal-sulfur batteries, like other materials with similar crystal structures previously researched for this purpose[35,36]. However, to the best of our knowledge, none of these applications of holey graphyne has been uncovered so far. Herein, we conducted a comprehensive study to explore its potential in thermoelectricity and H_2 production. By the presence of unique distinct bonding, κ_l is anticipated to be lower in holey graphyne compared to the other flat 2D materials from the graphene family, resulting in an enhanced thermoelectric figure of merit. On the other hand, variation in bond charge density accompanied by a highly porous plane, which increases the number of reactive sites, makes it an excellent choice for catalysis.

Computational details

The Vienna Ab-initio Simulation Package (VASP)[37,38] is used to perform the density functional theory (DFT) calculations by employing the Perdew – Burke – Ernzerhof and Heyd – Scuseria – Ernzerhof (HSE06) hybrid exchange–correlation functionals[39,40]. A plane wave cutoff energy of 550 eV and a Γ-centred *k*-mesh of $9\times9\times1$ ($30\times30\times1$) is used to sample the first Brillouin zone for self-consistent (non-self-consistent) calculations. The crystal is optimized until Hellmann–Feynman forces drop below 10^{-4} eV/Å. A vacuum of 15 Å, perpendicular to the sheet, is taken to eliminate the interactions between adjacent layers. The structural formation energy is calculated using $E_{form.} = (E_{tot.} - n.E_C)/n$ formula, where $E_{tot.}$ and E_C are the total energies of holey graphyne and an isolated C atom, respectively, and *n* is the total number of atoms in a unit cell. The phonon dispersion, thermal transport coefficients, and lattice thermal conductivity are calculated using the Hiphive[41], BoltzTraP2[42], and the ShengBTE[43] codes, respectively. This sophisticated method has been used to analyze the transport characteristics of numerous materials[44–46]. As inputs to ShengBTE, the 2nd and 3rd-order force constants are computed using a $3\times3\times1$ supercell. The 3rd-order force constants are calculated by displacing atoms up to the tenth nearest neighbors. A dense *q*-mesh $30\times30\times1$ is utilized to obtain well-converged lattice thermal conductivity. The produced lattice thermal conductivity is well converged, as the value at 300 K varies by less than 4% and 1% from the result obtained with displacing atoms up to the ninth nearest neighbors and $20\times20\times1$ *q*-mesh, respectively. The change in Gibbs free energy change (ΔG_H) is calculated using the relation, $\Delta G_H = \Delta E_H + \Delta E_{ZPE} - T\Delta S$, where ΔE_H, ΔE_{zpe}, T, and ΔS stand for the hydrogen adsorption energy, change in the zero-point energy, temperature (298.15 K), and change in entropy, respectively[47]. The value of $\Delta E_{ZPE} - T\Delta S$ is equal to 0.24 eV, giving rise to $\Delta G_H = \Delta E_H + 0.24$[47]. The adsorption energy of hydrogen is obtained as $\Delta E_H = E_{total} - E_{pristine} - 1/2E_{H2}$, where E_{total}, $E_{pristine}$, and E_{H2} are the total energies of holey graphyne with adsorbed H atom, pristine holey graphyne, and single H_2-molecule in the gas phase, respectively.

Results and discussions

Holey graphyne contains two rings comprised of six and eight carbon atoms, with a big pore, as shown in Fig. 1. Each primitive cell has an optimized in-plane lattice constant of 10.84 Å, in agreement with the previous study[33]. The C–C bonds have different bond lengths of 1.23 Å (*d1; sp* hybridized triple bond), 1.41 Å (*d2; sp* hybridized single bond), 1.40 Å (*d3;* sp^2 hybridized double bond), and 1.46 Å (*d4;* sp^2 hybridized single bond), as shown in Fig. 1b. The formation energy of holey graphyne is − 8.46 eV/atom, comparable to graphene (− 9.22 eV/atom) and *h*-BN (− 8.80 eV/atom) monolayers[48]. It is worthwhile to point out that holey graphyne has been experimentally synthesized using the bottom-up approach[33]. Besides that, *ab*-initio molecular dynamics simulations have determined that holey graphyne is thermally stable even at higher temperatures of 900 K.[33] Fig. 2 shows the

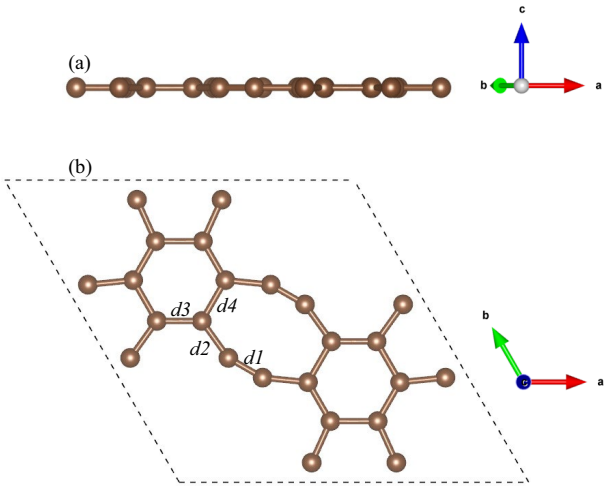

Figure 1. The side (**a**) and top (**b**) views of the optimized crystal structure of holey graphyne unit cell. di (i = 1–4) represents the bond length. Dashed lines enclose the unit cell.

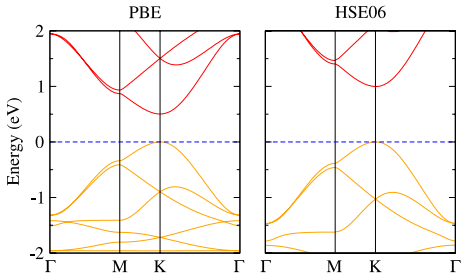

Figure 2. Calculated electronic band structures of holey graphyne. The orange and red curves correspond to valence and conduction bands, respectively. The blue dashed line represents the Fermi level.

calculated direct bandgaps of 0.50 eV (PBE) and 1.0 eV (HSE06), which agrees with the previously calculated value and is also close to the experimental value of 1.10 eV.[33].

The calculated phonon dispersion of holey graphyne has a total of 72 phonon modes without imaginary frequencies, assuring its dynamic stability (see Fig. 3). The out-of-plane flexural acoustic (ZA) phonons have the lowest frequency among the acoustic modes, followed by the in-plane transverse acoustic (TA) and longitudinal acoustic (LA) phonon modes. The first optical phonon mode has a noticeably small frequency of 2.55 THz, favoring the high phonon–phonon scattering owing to the coupling between ZA and the lowest optical phonons favors high phonon–phonon scattering[49,50]. Also, the less dispersive nature of optical phonons results in their small phonon group velocities. These distinct characteristics collectively contribute to low κ_l, compared to other carbon allotropes.

Figure 4 reveals the electronic transport coefficients with respect to varying carrier concentrations and temperatures. The electronic part of electrical (σ/τ) and thermal (κ_e/τ) conductivities increases and the Seebeck coefficient (S) declines linearly with carrier concentration[51]. The room temperature $|S|$ (300 μV/K at 1×10^{12} cm^{-2}) is approximately 6 times greater than that of graphene (~ 50 μV/K) at the same carrier concentration[52]. The p-type (n-type) $|S|$ turns out to be 114 μV/K (110 μV/K) even at the highest considered carrier concentration (2×10^{13} cm^{-2}) and at 600 K. The p-type $S^2\sigma/\tau$ rises with growing carrier concentration until it approaches 5×10^{11} W/mK^{2}s (9×10^{11} W/mK^{2}s) at 300 K (600 K) and then drops as the doping concentration elevates. Such a remarkably high S and $S^2\sigma/\tau$ suggest that investigating holey graphyne for thermoelectrics is worthwhile. It is further notable that identical dispersions of the valence band maxima and the conduction band minima result in similar variance in p-type and n-type electronic transport coefficients.

Further, we have looked into how lattice vibrations affect heat conduction in holey graphyne (see Fig. 5a). The calculated room temperature κ_l turns out to be 29.3 W/mK, lower than graphene (3000 W/mK)[53], γ-graphyne (76.4 W/mK)[54], C_3N (128 W/mK)[53], and C_2N (82.22 W/mK)[55]. The calculated κ_l at 300 K differs by 0.01% from the results obtained using $20\times20\times1$ q-mesh (i.e., 29.4 W/mK), leaving no relevant effect on our conclusion. The atom displacement to the ninth nearest neighbors yields κ_l of 28.05 W/mK, which deviates by 4% from the value obtained by displacing atoms up to the tenth nearest neighbors. The ultralow κ_l of holey graphyne, which is appealing from the thermoelectric perspective, is attributed to its bonds being less stiff than those of the above-mentioned flat materials. The C–C bond stiffness is determined by the spring constant (K) of holey graphyne, which is calculated as the trace of the harmonic force constant tensor between the closest adjacent atoms. It is written as $K = \Phi_{CC}^{xx} + \Phi_{CC}^{yy} + \Phi_{CC}^{zz}$, where $\Phi_{MX}^{\alpha\alpha}$ is the second derivate of energy with respect to displacement of atoms along the Cartesian axis α. The bond stiffness of *d1*, *d2*, *d3*, and *d4* are 87 eV/Å^2, 36 eV/Å^2, 44 eV/Å^2, and 31 eV/Å^2, which are substantially smaller than that of graphene (10,105 eV/Å^2). Such a bond feature inhibits heat transfer via lattice vibrations, leading to low κ_l values. Figure 5a shows that as temperature increases κ_l decreases due to the pronounced phonon–phonon scattering and follows the relation $\kappa_l \propto 1/T$.

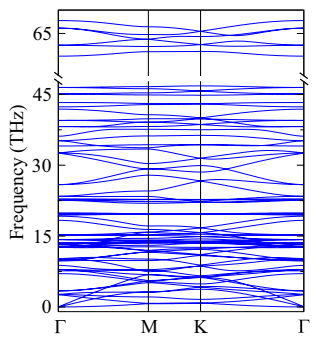

Figure 3. Calculated phonon dispersion of holey graphyne.

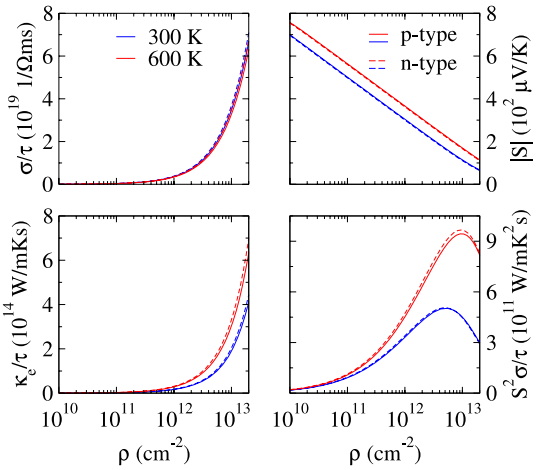

Figure 4. Calculated *p*-type and n-type electronic transport coefficients as a function of carrier concentration (ρ) at 300 K and 600 K.

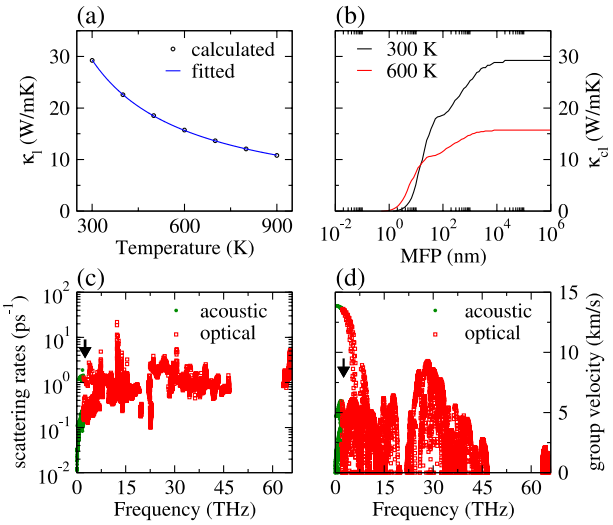

Figure 5. (**a**) Calculated and fitted ($\kappa_l \propto 1/T$) κ_l as a function of temperature, (**b**) cumulative lattice thermal conductivity (κ_{cl}) as a function of phonon mean free path (MFP), (**c**) phonon scattering rates, and (**d**) phonon group velocities at 300 K as a function of phonon frequency. The black arrows in (**c** and **d**) represent frequency 2.55 THz of first optical phonon mode at Γ point.

Nanostructuring of materials, where materials are composed of nanometer size grains and further with nanoscale internal structures[56], can reduce κ_l without affecting σ. To better comprehend the scope of phonon engineering, the cumulative lattice thermal conductivity (κ_{cl}) as a function of the phonon mean free path (MFP) is investigated and presented in Fig. 5b. As MFP decreases, the phonons scattering increases reducing the heat transfer. The contribution of phonons with different MFPs to lattice thermal conductivity is studied by calculating κ_{cl}, thereby deducing phonons most relevant to thermal conduction[43]. At 300 K (600 K) 75% of κ_l is by phonons having MFP 335 nm (110 nm), which implies reducing κ_l through nanostructuring is a viable strategy for holey graphyne. In other words, a sample size of 335 nm (110 nm) could help reduce the inherited value of κ_l at 300 K (600 K) by one-fourth. κ_{cl} increases (decreases) with rising MFP (temperature) and shows a plateau above 20,092 nm (7924 nm) at 300 K (600 K). A lower plateau at 600 K is due to the stronger phonon scattering at elevated temperatures[10]. Given that phonon transports are predominantly dependent on phonon scattering rates and phonon group velocities, our calculated results for acoustic and optical phonon modes are illustrated in Fig. 5c,d. The highest scattering rate for acoustic phonons at room temperature is 2.74 ps^{-1}, comparatively higher

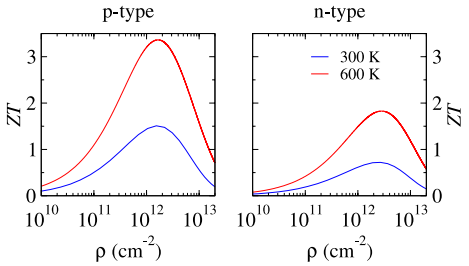

Figure 6. Calculated figure of merit (ZT) of holey graphyne.

than C_3N monolayer (2 ps^{-1})[53]. It is due to the coupling of acoustic and optical phonon modes, which leads to increased scattering rates of acoustic phonons, leading to a considerable reduction of κ_l[50]. The phonon group velocities are calculated to validate the above analysis and presented in Fig. 5d. The highest phonon group velocity of acoustic phonon mode at room temperature is 13.9 km/s, much lower than that of graphene (~ 22 km/s)[57] and nitrogenated holey graphene (18.48 km/s)[58]. Such low group velocity is a consequence of flat phonon modes (see Fig. 3)[50]. Thus, smaller κ_l of holey graphyne arises from low phonon group velocity and high scattering rates.

The figure of merit (*ZT*) depends on the relaxation time (τ) and is vital for showcasing the potential of a material for its thermoelectric applications. In this work, we have adapted the value for τ from the deformation potential theory used in the previous study[33]. The relation $\tau_T = 300^{*}\tau_{300}/T$ is engaged to yield its value at 600 K. The values of τ for holes (electrons) turn out to be 3.27 ps (1.16 ps) and 1.64 ps (0.58 ps) at 300 K and 600 K, respectively. The calculated *ZT* in Fig. 6 follows an upward trend similar to $S^2\sigma/\tau$. The *p*-type *ZT* is higher than the *n*-type and is counter to the trend seen in electronic transport coefficients (see Fig. 4). It is a result of the fact that holes and electrons have different relaxation times. The relation $ZT = S^2T/(\kappa_e/\sigma + \kappa_l/\sigma)$, where κ_l/σ is influenced by τ, explains that larger τ values result in greater *ZT*. The *ZT* secures peak values of 3.36 (1.50) and 1.82 (0.71) at 600 K (300 K) for *p*-type and *n*-type dopings, respectively. In the previous study[33], *ab*-initio molecular dynamics simulations determined that holey graphyne is thermally stable even at higher temperatures of 900 K, as established based on the ab initio molecular dynamics simulations. The room temperature *p*-type *ZT* of holey graphyne is higher than that of holey graphene (1.13)[59] and significantly higher than pristine graphene (0.55×10^{-3})[60] and γ-graphyne (0.48)[54].

Since active and cost-effective metal-free catalysts, as opposed to costly Pt-based catalysts, for HER are necessary to attain sustainable energy systems. We have also uncovered the response of holey graphyne to HER. As the standard descriptor for HER activity is the Gibbs free energy (ΔG_H), which is derived from the hydrogen adsorption energy. In the first instance, the H atom is adsorbed on all the possible 9 adsorption sites (s1–s9 in Fig. 7a). The H atom finds the s2 site the most favorable. The corresponding ΔG_H of s2 site is 0.20 eV, which is much smaller than that of graphene (1.41 eV)[61], phosphorene (1.25 eV)[62], and C_3N_4 (0.58 eV)[63] and comparable to biphenylene (0.29 eV)[61], see Fig. 7b. As a matter of fact, $\Delta G_H = 0$ stands out as an optimal value for HER. However, a value of $|\Delta G_H| < 0.2$ eV signifies the better catalytic performance of materials for HER activity[64]. We further engaged strain engineering to evaluate its impact on ΔG_H. It is observed that 2% compressive strain improves the catalytic performance of holey graphyne by reducing ΔG_H to 0.03 eV. Moreover, the-ab initio molecular dynamics simulation assures the thermal stability of hydrogen adsorbed holey graphyne concerning the low energy fluctuations alongside the intact H and the sheet structure after a time of 8 ps (see Fig. 7c). To address the photocatalytic performance of holey graphyne, the positions of valence band maxima (VBM) and conduction band minima (CBM) relative to the vacuum level along with H_+/H_2 reduction and (O_2/H_2O) oxidation potentials for water splitting are presented in Fig. 7d. It is evident that CBM is more positive than the H^+/H_2 potential, suggesting that holey graphyne is a potential material for photocatalytic hydrogen production. In contrast, the VBM is higher than the O_2/H_2O oxidation potential; hence, the holey graphene is unsuitable for oxidizing H_2O to O_2. However, an appropriate band engineering to shift the VBM downwards (e.g., doping, application of an external bias, heterojunction, etc.) may enable the water splitting into H_2 and O_2.

Conclusions

Using the first-principles computations, we investigated the thermal transport properties and HER catalytic activity of holey graphyne, a semiconducting material with a direct bandgap of 1.0 eV. The closely packed phonons display positive frequencies across the entire Brillouin zone, assuring the dynamic stability of holey graphyne. The room temperature |S| is as high as 300 μV/K at 1×10^{12} cm^{-2} (nearly sixfold than graphene). Flexural acoustic phonons couple with the lowest optical phonon mode to enhance phonon–phonon scattering and eventually decrease κ_l. The estimated room temperature κ_l of 29.3 W/mK is ultralow compared to that of graphene (3000 W/mK), attributed to its low bond stiffness. With the aid of nanostructure engineering, κ_l further reduces by a factor of four for a crystal size of around 335 nm (110 nm) at 300 K (600 K). The room temperature *p*-type *ZT* achieves a maximum value of 1.50, largely greater than graphene (0.55×10^{-3}), demonstrating its superior thermoelectric performance. Lastly, holey graphyne having low overpotential and more positive CBM than the H^+/H_2 potential, is also capable of catalyzing HER.

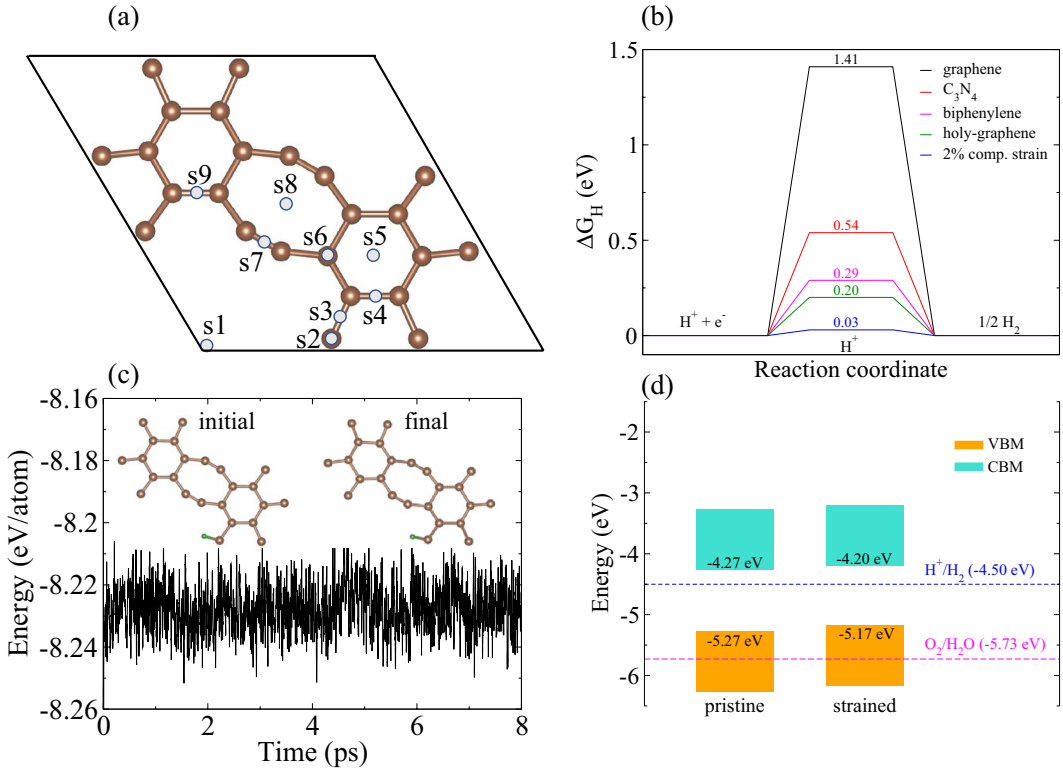

Figure 7. (**a**) The unit cell of holey graphyne with the possible adsorption sites (s1–s9) of hydrogen. (**b**) Calculated Gibbs free energy (ΔG_H) of hydrogen adsorption on holey graphyne. The corresponding values on graphene [Ref. [61]], C_3N_4 [Ref. [63]], and biphenylene [Ref. [61]] are also included for comparison. (**c**) The fluctuation of total energy during ab-initio molecular dynamics simulations at 300 K alongside the initial and the final hydrogen-adsorbed holey graphene structures. The brown and green spheres represent C and H atoms, respectively. (**d**) Calculated band edge positions of pristine and strained (2% compressive strain) holey graphene relative to the vacuum level.

Data availability

The datasets used and/or analysed during the current study available from the corresponding author on reasonable request.

Received: 14 March 2023; Accepted: 11 May 2023
Published online: 05 June 2023

References

1. Lewis, N. S. & Nocera, D. G. Powering the planet: Chemical challenges in solar energy utilization. *Proc. Natl. Acad. Sci.* **103**(43), 15729–15735. https://doi.org/10.1073/pnas.0603395103 (2006).
2. GSR2018_Full-Report_English.
3. Kverndokk, S. *Depletion of Fossil Fuels and the Impact of Global Warming*; Statistics Norway, Research Department: Oslo (1994). http://hdl.handle.net/10419/192091.
4. Kabeyi, M. J. B. & Olanrewaju, O. A. Sustainable energy transition for renewable and low carbon grid electricity generation and supply. *Front. Energy Res.* https://doi.org/10.3389/fenrg.2021.743114 (2022).
5. Dunn, S. Hydrogen futures: Toward a sustainable energy system. *Int J. Hydrog. Energy* **27**(3), 235–264. https://doi.org/10.1016/S0360-3199(01)00131-8 (2002).
6. Wu, H.-H. *et al.* Monolayer triphosphates MP_3 (M = Sn, Ge) with excellent basal catalytic activity for hydrogen evolution reaction. *Nanoscale* **11**(25), 12210–12219. https://doi.org/10.1039/C9NR03255J (2019).
7. Zhang, J., Sasaki, K., Sutter, E. & Adzic, R. R. Stabilization of platinum oxygen-reduction electrocatalysts using gold clusters. *Science (1979)* **315**(5809), 220–222. https://doi.org/10.1126/science.1134569 (2007).
8. Tymoczko, J., Calle-Vallejo, F., Schuhmann, W. & Bandarenka, A. S. Making the hydrogen evolution reaction in polymer electrolyte membrane electrolysers even faster. *Nat. Commun.* **7**(1), 10990. https://doi.org/10.1038/ncomms10990 (2016).
9. Sahoo, M. R., Ray, A. & Singh, N. Theoretical insights into the hydrogen evolution reaction on VGe_2N_4 and $NbGe_2N_4$ monolayers. *ACS Omega* **7**(9), 7837–7844. https://doi.org/10.1021/acsomega.1c06730 (2022).
10. *Recent Trends in Thermoelectric Materials Research II*; Semiconductors and semimetals ; v. 70; Academic Press: San Diego (2001).
11. Snyder, G. J. & Toberer, E. S. Complex thermoelectric materials. *Nat. Mater.* **7**(2), 105–114. https://doi.org/10.1038/nmat2090 (2008).
12. Pei, J., Cai, B., Zhuang, H.-L. & Li, J.-F. Bi2Te3-based applied thermoelectric materials: Research advances and new challenges. *Natl. Sci. Rev.* **7**(12), 1856–1858. https://doi.org/10.1093/nsr/nwaa259 (2020).
13. Novoselov, K. S. *et al.* Electric field effect in atomically thin carbon films. *Science (1979)* **306**(5696), 666–669. https://doi.org/10.1126/science.1102896 (2004).

14. Allen, M. J., Tung, V. C. & Kaner, R. B. Honeycomb carbon: A review of graphene. *Chem. Rev.* **110**(1), 132–145. https://doi.org/10.1021/cr900070d (2010).
15. Zhao, M., Dong, W. & Wang, A. Two-dimensional carbon topological insulators superior to graphene. *Sci. Rep.* **3**(1), 3532. https://doi.org/10.1038/srep03532 (2013).
16. Malko, D., Neiss, C., Viñes, F. & Görling, A. Competition for graphene: Graphynes with direction-dependent dirac cones. *Phys. Rev. Lett.* **108**(8), 086804. https://doi.org/10.1103/PhysRevLett.108.086804 (2012).
17. Zhang, X., Wei, L., Tan, J. & Zhao, M. Prediction of an ultrasoft graphene allotrope with dirac cones. *Carbon N. Y.* **105**, 323–329. https://doi.org/10.1016/j.carbon.2016.04.058 (2016).
18. Jiang, J.-W. *et al.* Twin graphene: A novel two-dimensional semiconducting carbon allotrope. *Carbon N. Y.* **118**, 370–375. https://doi.org/10.1016/j.carbon.2017.03.067 (2017).
19. Zhang, W., Chai, C., Fan, Q., Song, Y. & Yang, Y. Two-dimensional carbon allotropes with tunable direct band gaps and high carrier mobility. *Appl. Surf Sci.* **537**, 147885. https://doi.org/10.1016/j.apsusc.2020.147885 (2021).
20. Mahmood, J. *et al.* Nitrogenated holey two-dimensional structures. *Nat. Commun.* **6**, 4–10. https://doi.org/10.1038/ncomms7486 (2015).
21. Mahmood, J. *et al.* Two-dimensional polyaniline (C 3 N) from carbonized organic single crystals in solid state. *Proc. Natl. Acad. Sci.* **113**(27), 7414–7419. https://doi.org/10.1073/pnas.1605318113 (2016).
22. Fan, Q. *et al.* Nanoribbons with nonalternant topology from fusion of polyazulene: Carbon allotropes beyond graphene. *J. Am. Chem. Soc.* **141**(44), 17713–17720. https://doi.org/10.1021/jacs.9b08060 (2019).
23. Li, Y. *et al.* Architecture and electrochemical performance of alkynyl-linked naphthyl carbon skeleton: Naphyne. *ACS Appl. Mater. Interfaces* **12**(29), 33076–33082. https://doi.org/10.1021/acsami.0c05741 (2020).
24. Pan, Q. *et al.* Direct synthesis of crystalline graphtetrayne—a new graphyne allotrope. *CCS Chem.* **3**(4), 1368–1375. https://doi.org/10.31635/ccschem.020.202000377 (2021).
25. Fan, Q. *et al.* Biphenylene network: A nonbenzenoid carbon allotrope. *Science (1979)* **372**(6544), 852–856. https://doi.org/10.1126/science.abg4509 (2021).
26. Kim, B. G. & Choi, H. J. Graphyne: Hexagonal network of carbon with versatile dirac cones. *Phys Rev B* **86**(11), 115435. https://doi.org/10.1103/PhysRevB.86.115435 (2012).
27. Ouyang, T. *et al.* Systematic enumeration of low-energy graphyne allotropes based on a coordination-constrained searching strategy. *Phys. Status Solidi (RRL) Rapid Res. Lett.* **14**(12), 2000437. https://doi.org/10.1002/pssr.202000437 (2020).
28. Kou, J., Zhou, X., Lu, H., Wu, F. & Fan, J. Graphyne as the membrane for water desalination. *Nanoscale* **6**(3), 1865–1870. https://doi.org/10.1039/C3NR04984A (2014).
29. Yan, P. *et al.* Newly discovered graphyne allotrope with rare and robust dirac node loop. *Nanoscale* **13**(6), 3564–3571. https://doi.org/10.1039/D0NR08397F (2021).
30. Ouyang, T. *et al.* Thermoelectric properties of gamma-graphyne nanoribbons and nanojunctions. *J. Appl. Phys.* **114**(7), 073710. https://doi.org/10.1063/1.4818616 (2013).
31. Panigrahi, P. *et al.* Two-dimensional nitrogenated holey graphene (C2N) monolayer based glucose sensor for diabetes mellitus. *Appl. Surf. Sci.* **2021**(573), 151579. https://doi.org/10.1016/j.apsusc.2021.151579 (2021).
32. Sajjad, M., Hussain, T., Singh, N. & Larsson, J. A. Superior anchoring of sodium polysulfides to the polar C2N 2D material: A potential electrode enhancer in sodium-sulfur batteries. *Langmuir* **36**(43), 13104–13111. https://doi.org/10.1021/acs.langmuir.0c02616 (2020).
33. Liu, X. *et al.* Constructing two-dimensional holey graphyne with unusual annulative π-extension. *Matter* https://doi.org/10.1016/j.matt.2022.04.033 (2022).
34. James, A. *et al.* Graphynes: Indispensable nanoporous architectures in carbon flatland. *RSC Adv.* **8**(41), 22998–23018. https://doi.org/10.1039/C8RA03715A (2018).
35. Al-Jayyousi, H. *et al.* Exploring the superior anchoring performance of the two-dimensional nanosheets $B_2C_4P_2$ and $B_3C_2P_3$ for lithium-sulfur batteries. *ACS Omega* **7**(43), 38543–38549. https://doi.org/10.1021/acsomega.2c03898 (2022).
36. Al-Jayyousi, H. K., Sajjad, M., Liao, K. & Singh, N. Two-dimensional biphenylene: A promising anchoring material for lithium-sulfur batteries. *Sci. Rep.* **12**(1), 4653. https://doi.org/10.1038/s41598-022-08478-5 (2022).
37. Kresse, G. & Furthmüller, J. Efficiency of Ab-initio total energy calculations for metals and semiconductors using a plane-wave basis set. *Comput. Mater. Sci.* **6**(1), 15–50. https://doi.org/10.1016/0927-0256(96)00008-0 (1996).
38. Kresse, G. & Furthmüller, J. Efficient iterative schemes for Ab initio total-energy calculations using a plane-wave basis set. *Phys. Rev. B* **54**(16), 11169–11186. https://doi.org/10.1103/PhysRevB.54.11169 (1996).
39. Perdew, J. P., Burke, K. & Ernzerhof, M. Generalized gradient approximation made simple. *Phys. Rev. Lett.* **77**(18), 3865–3868. https://doi.org/10.1103/PhysRevLett.77.3865 (1996).
40. Krukau, A. V., Vydrov, O. A., Izmaylov, A. F. & Scuseria, G. E. Influence of the exchange screening parameter on the performance of screened hybrid functionals. *J. Chem. Phys.* **125**(22), 224106. https://doi.org/10.1063/1.2404663 (2006).
41. Eriksson, F., Fransson, E. & Erhart, P. The hiphive package for the extraction of high-order force constants by machine learning. *Adv. Theory Simul.* **2**(5), 1800184. https://doi.org/10.1002/adts.201800184 (2019).
42. Madsen, G. K. H., Carrete, J. & Verstraete, M. J. BoltzTraP2, a program for interpolating band structures and calculating semi-classical transport coefficients. *Comput. Phys. Commun.* **231**, 140–145. https://doi.org/10.1016/j.cpc.2018.05.010 (2018).
43. Li, W., Carrete, J., Katcho, A. & Mingo, N. ShengBTE: A solver of the boltzmann transport equation for phonons. *Comput. Phys. Commun.* **185**(6), 1747–1758. https://doi.org/10.1016/j.cpc.2014.02.015 (2014).
44. Wang, B., Yan, X., Cui, X. & Cai, Y. First-principles study of the phonon lifetime and low lattice thermal conductivity of monolayer γ-GeSe: A comparative study. *ACS Appl. Nano Mater.* **5**(10), 15441–15448. https://doi.org/10.1021/acsanm.2c03476 (2022).
45. Shu, Z. *et al.* High-performance thermoelectric monolayer γ-GeSe and its group-IV monochalcogenide isostructural family. *Chem. Eng. J.* **454**, 140242. https://doi.org/10.1016/j.cej.2022.140242 (2023).
46. Sajjad, M. & Singh, N. The impact of electron-phonon coupling on the figure of merit of Nb_2SiTe_4 and Nb_2GeTe_4 ternary monolayers. *Phys. Chem. Chem. Phys.* **23**(29), 15613–15619 (2021).
47. Nørskov, J. K. *et al.* Trends in the exchange current for hydrogen evolution. *J. Electrochem. Soc.* **152**(3), J23. https://doi.org/10.1149/1.1856988 (2005).
48. Mortazavi, B., Shojaei, F., Yagmurcukardes, M., Shapeev, A. V. & Zhuang, X. Anisotropic and outstanding mechanical, thermal conduction, optical, and piezoelectric responses in a novel semiconducting BCN monolayer confirmed by first-principles and machine learning. *Carbon N. Y.* **200**, 500–509. https://doi.org/10.1016/j.carbon.2022.08.077 (2022).
49. Mann, S. *et al.* Lattice thermal conductivity of pure and doped (B, N) Graphene. *Mater. Res. Express* https://doi.org/10.1088/2053-1591/abb2cd (2020).
50. Morelli, D. T. & Slack, G. A. High lattice thermal conductivity solids. *High Therm. Conduct. Mater.* **37**, 68. https://doi.org/10.1007/0-387-25100-6_2 (2006).
51. Li, L., Meller, G. & Kosina, H. Analytical conductivity model for doped organic semiconductors. *J. Appl. Phys.* https://doi.org/10.1063/1.2472282 (2007).
52. Ali, M., Pi, X., Liu, Y. & Yang, D. Electronic and thermoelectric properties of atomically thin C_3Si_3/C and C_3Ge_3/C superlattices. *Nanotechnology* https://doi.org/10.1088/1361-6528/aa9ebb (2018).

53. Kumar, S., Sharma, S., Babar, V. & Schwingenschlögl, U. Ultralow lattice thermal conductivity in monolayer C3N as compared to graphene. *J. Mater. Chem. A Mater.* **5**(38), 20407–20411. https://doi.org/10.1039/c7ta05872a (2017).
54. Jiang, P. H. *et al.* Thermoelectric properties of γ-graphyne from first-principles calculations. *Carbon N. Y.* **113**, 108–113. https://doi.org/10.1016/j.carbon.2016.11.038 (2017).
55. Ouyang, T. *et al.* First-principles study of thermal transport in nitrogenated holey graphene. *Nanotechnology* https://doi.org/10.1088/1361-6528/28/4/045709 (2017).
56. Singh, D. J. & Terasaki, I. Thermoelectrics: Nanostructuring and more. *Nat. Mater.* **7**(8), 616–617. https://doi.org/10.1038/nmat2243 (2008).
57. Mortazavi, B. *et al.* Efficient machine-learning based interatomic potentialsfor exploring thermal conductivity in two-dimensional materials. *J. Phys. Mater.* https://doi.org/10.1088/2515-7639/ab7cbb (2020).
58. Zhao, Y., Dai, Z., Lian, C. & Meng, S. Exotic thermoelectric behavior in nitrogenated holey graphene. *RSC Adv.* **7**(42), 25803–25810. https://doi.org/10.1039/c7ra03597g (2017).
59. Singh, D., Shukla, V. & Ahuja, R. Optical excitations and thermoelectric properties of two-dimensional holey graphene. *Phys. Rev. B* **102**(7), 75444. https://doi.org/10.1103/PhysRevB.102.075444 (2020).
60. Anno, Y., Imakita, Y., Takei, K., Akita, S. & Arie, T. Enhancement of graphene thermoelectric performance through defect engineering. *2d Mater.* https://doi.org/10.1088/2053-1583/aa57fc (2017).
61. Luo, Y. *et al.* A first principles investigation on the structural, mechanical, electronic, and catalytic properties of biphenylene. *Sci. Rep.* **11**(1), 1–6. https://doi.org/10.1038/s41598-021-98261-9 (2021).
62. Cai, Y. *et al.* Design of phosphorene for hydrogen evolution performance comparable to platinum. *Chem. Mater.* **31**(21), 8948–8956. https://doi.org/10.1021/acs.chemmater.9b03031 (2019).
63. Zheng, Y. *et al.* Hydrogen evolution by a metal-free electrocatalyst. *Nat. Commun.* **5**(1), 3783. https://doi.org/10.1038/ncomms4783 (2014).
64. Huang, B., Zhou, N., Chen, X., Ong, W. & Li, N. Insights into the electrocatalytic hydrogen evolution reaction mechanism on two-dimensional transition-metal carbonitrides (MXene). *Chem. A Eur. J.* **24**(69), 18479–18486. https://doi.org/10.1002/chem.201804686 (2018).

Acknowledgements

N.S acknowledges the financial support from Khalifa University of Science and Technology under the Emerging Science & Innovation Grant ESIG-2023-004. The authors also acknowledge the contribution of Khalifa University's high-performance computing and research computing facilities to the results of this research.

Author contributions

M.S. and S.S.N. performed the calculations and wrote the original draft. Y.A.S. reviewed and edited the manuscript. N.S. created the idea and supervised the project and finally reviewed the manuscript.

Competing interests

The authors declare no competing interests.

Additional information

Correspondence and requests for materials should be addressed to N.S.

Reprints and permissions information is available at www.nature.com/reprints.

Publisher's note Springer Nature remains neutral with regard to jurisdictional claims in published maps and institutional affiliations.